NeuroImage 53 (2010) 139–145

Contents lists available at ScienceDirect

NeuroImage

journal homepage: www.elsevier.com/locate/ynimg

Prospective motion correction of high-resolution magnetic resonance imaging data in children

Timothy T. Brown [a,b,*], Joshua M. Kuperman [a,c], Matthew Erhart [a,b], Nathan S. White [a,c], J. Cooper Roddey [a,c], Ajit Shankaranarayanan [d], Eric T. Han [d], Dan Rettmann [e], Anders M. Dale [a,b,c]

[a] Multimodal Imaging Laboratory, University of California, San Diego, La Jolla, CA, USA
[b] Department of Neurosciences, University of California, San Diego, La Jolla, CA, USA
[c] Department of Radiology, University of California, San Diego, La Jolla, CA, USA
[d] Applied Science Laboratory, GE Healthcare, Menlo Park, CA, USA
[e] Applied Science Laboratory, GE Healthcare, Rochester, MN, USA

ARTICLE INFO

Article history:
Received 17 April 2010
Revised 29 May 2010
Accepted 6 June 2010
Available online 11 June 2010

ABSTRACT

Motion artifacts pose significant problems for the acquisition and analysis of high-resolution magnetic resonance imaging data. These artifacts can be particularly severe when studying pediatric populations, where greater patient movement reduces the ability to clearly view and reliably measure anatomy. In this study, we tested the effectiveness of a new prospective motion correction technique, called PROMO, as applied to making neuroanatomical measures in typically developing school-age children. This method attempts to address the problem of motion at its source by keeping the measurement coordinate system fixed with respect to the subject throughout image acquisition. The technique also performs automatic rescanning of images that were acquired during intervals of particularly severe motion. Unlike many previous techniques, this approach adjusts for both in-plane and through-plane movement, greatly reducing image artifacts without the need for additional equipment. Results show that the use of PROMO notably enhances subjective image quality, reduces errors in Freesurfer cortical surface reconstructions, and significantly improves the subcortical volumetric segmentation of brain structures. Further applications of PROMO for clinical and cognitive neuroscience are discussed.

Introduction

Artifacts caused by head and body motion pose a significant problem for the *in vivo* magnetic resonance imaging (MRI) of the human brain. Motion artifacts adversely affect the ability to accurately characterize the size, shape, and tissue properties of brain structures in both research subjects and clinical patients. In cognitive neuroscience applications, cross-sectional and longitudinal effects in neuroanatomical measurements are relatively small, making them easily obscured by distortions arising from patient and subject movement. In addition to lowering sensitivity, motion can also introduce systematic bias into statistical comparisons, since groups are commonly defined according to behavioral, clinical, and developmental variables that relate to differing levels of movement during data collection (Blumenthal and Zijdenbos, 2002; Brown et al., 2006; Jezzard and Clare, 1999).

While all subject populations are susceptible to motion artifacts, these problems are particularly pronounced with children, who frequently have difficulty remaining still throughout the time required for high-resolution image acquisition (Byars et al., 2002; Davidson et al., 2003; Poldrack et al., 2002; Wilke et al., 2003). Although sedation can be justified with clinical pediatric populations in order to obtain diagnostically useful MRI data, it comes with risks and adds to the cost, invasiveness, and inconvenience of the procedures for children and their parents (Malviya et al., 1997; Ronchera-Oms et al., 1994; Voepel-Lewis et al., 2000). In addition, sedation is generally untenable with healthy child and adult research participants.

The nature and magnitude of MRI artifacts, as well as the efficacy of correction methods, depend greatly on which specific pulse sequences are being used. In two-dimensional single shot sequences, between-scan movement causes image distortions mainly by introducing changes in the spin excitation history of the acquisition. In multi-shot two- and three-dimensional pulse sequences, motion can be even more problematic, as k-space data inconsistencies cause ringing artifacts, ghosting, and blurring of the boundaries between structures of interest.

Among the various methods currently available for limiting the severity of motion-induced artifacts, there are tradeoffs and limitations regarding the feasibility, effectiveness, and equipment requirements. Although many between-volume distortions can be dealt with

* Corresponding author. 8950 Villa La Jolla Drive, Suite C-101, La Jolla, CA 92093-0841, USA. Fax: +1 858 534 1078.
E-mail address: ttbrown@ucsd.edu (T.T. Brown).

1053-8119/$ – see front matter © 2010 Elsevier Inc. All rights reserved.
doi:10.1016/j.neuroimage.2010.06.017

effectively using offline image registration approaches (Cox and Jesmanowicz, 1999; Friston et al., 1995; Jenkinson and Smith, 2001; Woods et al., 1998), it is difficult to correct retrospectively for motion-induced artifacts. Post-hoc correction of within-volume artifacts is problematic and requires precise k-space interpolation and grid readjustment in order to accurately reconstruct the images (Kochunov et al., 2006; Liu et al., 2004; Manduca et al., 2000; Pipe, 1999). Although these approaches have been shown to mitigate many different types of motion-related artifacts, they cannot correct for motion that occurs orthogonal to the plane of image acquisition. In addition, all retrospective movement correction methods introduce some degree of blurring or image distortion due to interpolation.

An alternative approach to motion artifact correction is to modify the pulse sequence during the course of the acquisition itself, in real time. Such prospective motion correction methods attempt to keep the coordinate system fixed with respect to the patient throughout the scanning process, thereby avoiding the need for post-hoc image interpolation. Prospective correction methods have commonly used navigator scans with a variety of k-space trajectory shapes, including linear (Firmin and Keegan, 2001; Norris and Driesel, 2001; Weih et al., 2004), circular (Fu et al., 1995; Ward et al., 2000), spherical (Irarrazabal and Nishimura, 1995; Welch et al., 2002; Wong and Roos, 1994), and "cloverleaf"-shaped navigators (van der Kouwe et al., 2006), with varying degrees of speed and accuracy for tracking sophisticated types of motion in three dimensions. Other recently developed prospective methods have used optical monitoring to provide rapid, slice-wise correction of motion, but these approaches require elaborate additional hardware such as a mounted camera system and patient bite bar, as well as additional calibration procedures (Speck et al., 2006; Zaitsev et al., 2006).

In this paper, we present the application of a new image-based approach for prospective motion correction in MRI, called PROMO, which uses spiral navigator scans to perform real-time rigid-body motion tracking and correction (White et al., 2010). These navigators, which are interspersed within the dead time of standard image acquisition, are used to keep the coordinate system fixed relative to patient brain position, correcting for both in-plane and through-plane movement. In addition, PROMO uses non-iterative recursive filters that are well suited to rapid real-time implementation. This allows the technique to combine current position information with motion trajectory data to predict the position of the patient in the upcoming acquisition and to automatically rescan images that were acquired during intervals where significant head motion was detected.

Because child subjects generally show a greater degree of head motion in MRI than adults, we tested the effectiveness of PROMO naturalistically in a group of school-age children using outcome variables typically of interest to researchers in cognitive neuroscience. Specifically, we measured the ability of PROMO to enhance subjective image quality, reduce failures in cortical surface reconstructions, and improve the reliability of quantitative measures of subcortical volumetric segmentations made using the publicly available, automated Freesurfer algorithms.

Methods

Subjects

Nine healthy school-age children (mean = 10.73 years, SD = 0.54, range 9.9 to 11.6 years; three female) were recruited and screened by parental interview and questionnaire to rule out history of head injury, neurological or psychiatric disorder, and major medical problems. Parental informed consent and child assent was obtained in accordance with the UCSD Human Research Protections Program. All participants were screened for MRI safety by parent report and metal detector. Children were asked to remain still throughout data collection. During data acquisition, children viewed and listened to a DVD of their choice using a back-screen projection system, a mirror mounted on the head coil, and MRI-compatible headphones (MR Confon, Germany).

Image acquisition

Imaging data were obtained at the UCSD Radiology Imaging Laboratory on a 1.5 Tesla GE Signa HDx 14.0M5 TwinSpeed system (GE Healthcare, Waukesha, WI) using an eight-channel phased array head coil. Acquisitions included a conventional three-plane scout and a set of four 3D inversion recovery spoiled gradient echo (IR-SPGR) T1-weighted volumes with pulse sequence parameters optimized for maximum gray/white matter contrast (TE = 3.9 ms, TR = 8.7 ms, TI = 270 ms, flip angle = 8°, TD = 750 ms, bandwidth = ±15.63 kHz, FOV = 24 cm, matrix = 192 × 192, voxel size = 1.25 × 1.25 × 1.2 mm). The sequences used for the four T1 images were identical except that PROMO motion tracking and correction was turned off for two scans and on for the other two, in alternating fashion. The order of scanning for the four T1 scans was counterbalanced across subjects, with four participants undergoing a sequence of on–off–on–off and five undergoing off–on–off–on.

Real-time motion tracking and correction with spiral navigator (S-NAV) sequences was performed using the extended Kalman filter (EKF) algorithm (Gelb, 1974) applied to MRI as reported by Dale and colleagues (White et al., 2007, 2010) and as described previously for prospective motion correction in S-NAV 3D pulse sequences (Roddey et al., 2008; Shankaranarayanan et al., 2007). Five sets of three orthogonal low flip, single shot S-NAVs were interspersed within the dead time of all four 3D IR-SPGR T1 scans in order to measure and adjust for head movement while scanning (White et al., 2010). Of note, the placement of the S-NAV scans can vary according to the specific pulse sequence being used. Online navigator-derived motion measures were used to adjust the image coordinate system with respect to brain position and to automatically rescan images that were acquired during intervals with particularly high motion, as determined by the position difference between the two navigator scans that "sandwich" each partition. For this study, a rescan threshold was determined based on the noise level characteristics of a sample of "cooperative" adult subjects (i.e., who showed a relative absence of motion). Rescans were set to be triggered by a norm of 1 or greater in the motion measures during an acquisition (i.e., a norm of 1 mm of total translation or a norm of 1° of total rotation by any combination of the head position values; see White et al., 2010). A rescan of the entire volume was allowed, if necessary according to subject movement. For images acquired without PROMO, scan duration was 8 min, 40 s per T1 volume. The S-NAV/EKF framework offers the advantage of image-based tracking within regions of interest that are specific to each subject, masking out motion from non-brain locations such as the neck and jaw, which can corrupt the motion estimates.

Motion estimates for the PROMO-enabled volumes were computed from navigator scans, tracking position as a six-element vector. As an index of each individual's magnitude of head motion, the norm of the range of motion measures (minimum to maximum) was computed across both PROMO-on scans for each subject for translation and rotation. This "Euclidean" (or L2) norm is a normalized measure of the magnitude of variability in motion—in this case the square root of the sum of squares of the range of motion—that has the advantage of being independent of relative position in the x, y, z coordinate space. Motion estimates were not calculated for the two PROMO-off scans, since tracking and correction was disabled.

Image processing, reconstruction, and segmentation

Image files in DICOM format were transferred to a Linux workstation for viewing, rating, and automated cortical reconstruction and subcortical volumetric segmentation. The four T1-weighted

volumes were rigid-body registered to each other and realigned into a common stereotactic space. Heterogeneities in image intensity were corrected online using GE's calibration normalization procedure as well as offline using the FreeSurfer software suite (version 3.0.5; http://surfer.nmr.mgh.harvard.edu). Gradient coil nonlinear warping was corrected using tools developed through the Biomedical Informatics Research Network on morphometry (mBIRN).

Automated procedures for cortical surface-based reconstruction and subcortical volumetric segmentation were conducted. For each subject, MRI scans were used to construct a three-dimensional model of the cortical surface that includes: (1) segmentation of the white matter; (2) tessellation of the gray/white matter boundary; (3) inflation of the folded, tessellated surface; and (4) correction of topological defects. This multi-step procedure has been described in detail previously (Dale et al., 1999; Fischl et al., 1999, 2001). Measures of cortical thickness are obtained from this surface reconstruction by estimating and then refining the gray/white boundary, deforming the surface outward to the pial surface, and measuring the distances from each point on the white matter surface to the pial surface (Fischl and Dale, 2000). For the purposes of the current study, cortical thickness measurements were not compared between motion-corrected and uncorrected images, since artifacts in the uncorrected scans caused significant errors in the delineation of the surfaces by the automated reconstruction operation, rendering quantitative thickness comparisons meaningless. So, instead we report simply the number of surface reconstruction failures.

Volumetric subcortical segmentation and measurement was also performed using automated procedures that have been validated as comparable in accuracy to much slower, labor-intensive manual tracing and labeling methods (Fischl et al., 2002). This procedure automatically classifies brain tissue into multiple distinct structures such as cerebral and cerebellar gray and white matter, cerebrospinal fluid (CSF), caudate nucleus, hippocampus, and thalamus. Using probabilistic information derived from a manually labeled training data set, this approach automatically assigns a neuroanatomical label to each voxel in the MRI volume. First, data are rigid-body registered and morphed nonlinearly into a standard stereotactic space. Then, previously manually segmented images are used to calculate statistics about how likely a particular label is at any given location throughout the brain, and these data are used as Bayesian priors for estimating voxel identity in a given subject's brain. Three kinds of information are used by the segmentation to help disambiguate anatomical labels: (1) the prior probability of a given tissue class occurring at a specific location in the atlas space; (2) the image intensity likelihood given that tissue class; and (3) the probability of the local spatial configuration of the labels given the tissue class. Typically, all segmentations produced by this procedure are visually inspected for accuracy and may be edited prior to inclusion in research analyses. For the purposes of comparing motion-corrected and uncorrected images, however, segmentation results for all volumes were included in analyses without additional editing.

Image quality ratings and analyses

All four high-resolution T1-weighted volumes for each of the nine children were rated for overall image quality by an experienced neuroimaging technician who was blind to PROMO status (on versus off), subject number, and acquisition order. For these ratings, the expert viewed all image slices in the sagittal plane and judged the overall quality of the image volume according to global contrast properties and clarity. All 36 volumes were given a rating of 1, 2, or 3 (1 = good, 2 = adequate, 3 = poor). Images were also then inspected and rated specifically for common signs of subject head motion such as ghosting, blurring, and ring artifacts. For these blind ratings, the expert judged each volume according to a five-point scale ranging from 1 (no visible motion artifacts) to 5 (severe motion artifacts).

Table 1
Age and norm of motion range for PROMO-on scans by subject.

Subject	Age (years)	Translation (mm)	Rotation (°)
1	10.7	3.9	5.0
2	10.9	10.7	12.0
3	10.7	6.5	5.8
4	11.5	7.5	15.0
5	10.5	3.3	5.5
6	10.3	10.5	9.2
7	11.6	2.0	5.1
8	9.9	2.1	2.9
9	10.5	2.6	2.4

Automated cortical surface reconstructions were also performed for each of the 36 image volumes, and these were tallied for the number that successfully completed versus failed.

In order to test the reliability of the automated segmentation results, we computed for each subject the percent volume overlap between the two PROMO-on scans as well as between the two PROMO-off scans, for all structures of interest labeled morphometrically (Fischl et al., 2002). Comparing the two independent segmentation results for a given structure, the computed percent volume overlap yields a maximum value of 100 for identical segmentation results and decreasing values indicating less voxel-by-voxel overlap between the two segmentation labelings. Since many studies are primarily interested in quantifying volumetric differences and changes in structures, we also tested the reliability of volumetric measures without regard to spatial position overlap. For all regions of interest, we compared the difference between the two PROMO-on scans to the difference between the two PROMO-off scans, normalized by the mean volume of all four scans for that structure or ROI, independent of spatial position between scans (Fischl et al., 2002).

Results

Participant motion during scanning showed relatively large magnitude movements during the PROMO-on scans and varied considerably by individual, typical of school-age children (Table 1). The norm of the head motion ranges spanned from about 2 mm translation and 2° of rotation to more than a centimeter of translation and 15° of rotation, depending on the individual. The correlation coefficient (Pearson, two-tailed) between age and translation was $r = 0.08$ ($p = 0.83$) and between age and rotation was $r = 0.51$ ($p = 0.16$) in this small sample with a narrow age range.

Table 2
Number of rescans and added scan duration (+) for PROMO-on scans by subject, with descriptive statistics. Duration for PROMO-off scans was 520 s (8 min, 40 s).

PROMO-on 1			PROMO-on 2	
Subject	Rescans	± (s)	Rescans	± (s)
1	1	2.5	5	12.5
2	38	95	117	292.5
3	8	20	12	30
4	7	17.5	23	57.5
5	3	7.5	1	2.5
6	3	7.5	23	57.5
7	2	5	1	2.5
8	0	0	1	2.5
9	1	2.5	1	2.5
Per volume		Rescans		± (s)
Mean		13.7		34.3
Median		3		7.5
SD		27.8		69.4
Range		0–117		0–292.5

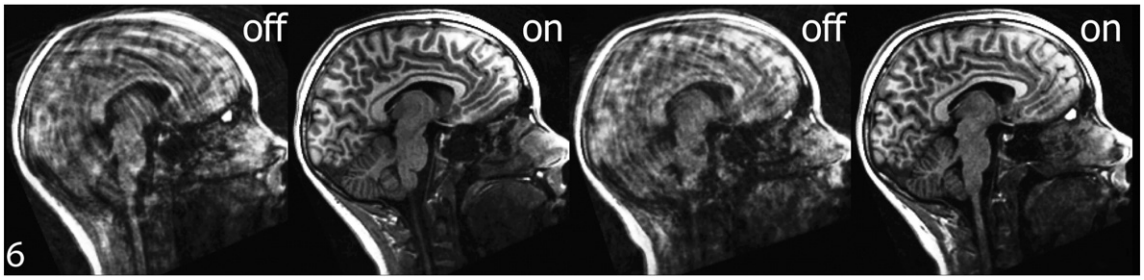

Fig. 1. T1-weighted midsagittal images by PROMO status for one subject. Reconstructed images for subject number six, comparing 3D IR-SPGR scans with PROMO off versus on, show greater image clarity and reduced blurring, ringing, and ghosting for both acquisitions using PROMO correction.

The number of rescans required because of subject movement, and therefore the additional time required for acquisition with PROMO enabled, also varied considerably among subjects (Table 2). The additional acquisition time required for PROMO-on scans was on average 34.3 s per volume, but this varied widely and was heavily affected by one outlying individual; the median additional scan time was 7.5 s, the standard deviation was 69.4 s, and the duration ranged from 0 to 292.5 s (4 min, 52.5 s). The correlation coefficient (Pearson, one-tailed) between the total number of rescans and head translation was $r=0.72$ ($p=0.01$) and between rescans and rotation was $r=0.61$ ($p=0.04$).

By blind ratings, T1-weighted volumes acquired when PROMO was enabled consistently showed better image quality in terms of clarity of structural boundaries, contrast properties, and lack of apparent motion artifacts. For example, the midsagittal image slice for each subject showed generally more blurring, ghosting, and ring artifacts in the PROMO-off scans than in the PROMO-on scans (Fig. 1, Fig. S1). Overall image quality ratings made slice-by-slice for the entire volumes were significantly better for images acquired with PROMO enabled versus disabled (Table 3; Mann–Whitney $U=36.5$, one-tailed, $p<0.0001$). Fifteen of the 18 PROMO-on volumes were rated as "good", whereas 11 of the 18 PROMO-off volumes were rated as "poor." When examined specifically for motion artifacts, PROMO-acquired images also showed superior ratings (Table 4; Mann–Whitney $U=34.0$, one-tailed, $p<0.0001$). Thirteen of the 18 PROMO-on volumes were rated as showing no visible motion artifacts, where by comparison, images acquired without PROMO were most frequently rated as showing moderate to severe levels of subject movement.

Automated cortical surface reconstructions and subcortical volumetric segmentations were both greatly improved by using prospective motion correction. The algorithm for automated surface reconstruction successfully completed in a greater proportion of the PROMO-on images, delineating the white matter, gray/white boundary, and pial surfaces in 16 of the 18 volumes (Table 5; Mann–Whitney $U=81.0$, one-tailed, $p<0.001$). By contrast, without motion correction only seven of the 18 surface reconstructions successfully completed.

Subcortical volumetric segmentation and measurement was also greatly improved with the use of correction in terms of the reliability of the spatial percent volume overlap of specific brain structures that were classified. Similar improvements were observed in the volume measurements that were made across scans, independent of position. For example, inspection of color-coded segmentation results in the coronal plane through the basal ganglia showed notably fewer tissue classification mistakes, border errors, and structure mislabelings in the PROMO-on scans relative to the PROMO-off scans (Fig. 2, Fig. S2). In addition, regional volumes acquired when motion correction was enabled showed less variability and higher percent volume overlap between scans than volumes acquired without correction (Fig. 3, Table S1). With motion correction disabled, percent volume overlap between scans was especially poor for cerebellar white matter and cerebellar gray matter measurements. By permutation tests, p-values of the differences between corrected and uncorrected image overlaps were: thalamus (0.06), caudate (0.02), putamen (0.01), pallidum (0.03), hippocampus (0.02), cerebral white matter (<0.01), cerebral gray matter (<0.01), ventricle (0.04), cerebellar white matter (0.03), cerebellar gray matter (0.04), and total brain (<0.01).

Volumetric measurements independent of spatial position showed consistently greater variability in the PROMO-off scans relative to the PROMO-on scans, as well as larger average between-scan volume differences for every ROI (Fig. 4, Table S2). Similar to the poor findings for percent volume overlap, cerebellar white and gray matter showed particularly large differences in volumetric measurements between motion-corrected and uncorrected data. P-values of the percent volume differences, as yielded by permutation tests, were: thalamus (0.71), caudate (0.94), putamen (0.05), pallidum (0.14), hippocampus (0.09), cerebral white matter (0.21), cerebral gray matter (0.01), ventricle (0.37), cerebellar white matter (0.06), cerebellar gray matter (0.02), and total brain (0.18).

Table 4
Image motion artifact ratings by PROMO status.

Rating	None		Mod		Severe	Total
	1	2	3	4	5	
PROMO						
On	13	4	0	1	0	18
Off	2	2	3	4	7	18
Total	15	6	3	5	7	36

Mann-Whitney $U=34.0$, $p<0.0001$ (one-tailed).

Table 3
Overall image quality ratings by PROMO status.

Rating	1/Good	2/Adeq	3/Poor	Total
PROMO				
On	15	2	1	18
Off	2	5	11	18
Total	17	7	12	36

Mann–Whitney $U=36.5$, $p<0.0001$ (one-tailed).

Table 5
Cortical surface reconstructions by PROMO status.

Reconstruction	Succeeded	Failed	Total
PROMO			
On	16	2	18
Off	7	11	18
Total	23	13	36

Mann–Whitney $U=81.0$, $p<0.001$ (one-tailed).

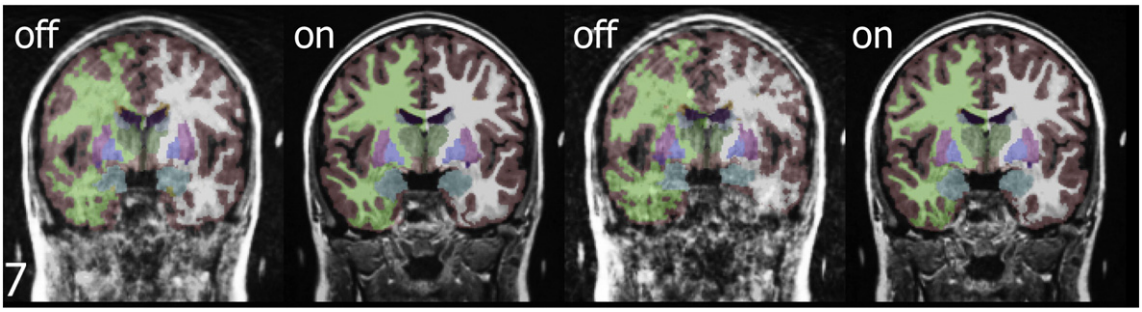

Fig. 2. Segmentation results by PROMO status for one subject. Reconstructed images for subject number seven, comparing color-coded segmentation results with PROMO off versus on, show improved delineation of anatomical structures such as gray matter (color = gray), white matter (light green), caudate head (dark green), putamen (magenta), pallidum (light blue), and amygdala (aquamarine) for both acquisitions using PROMO correction.

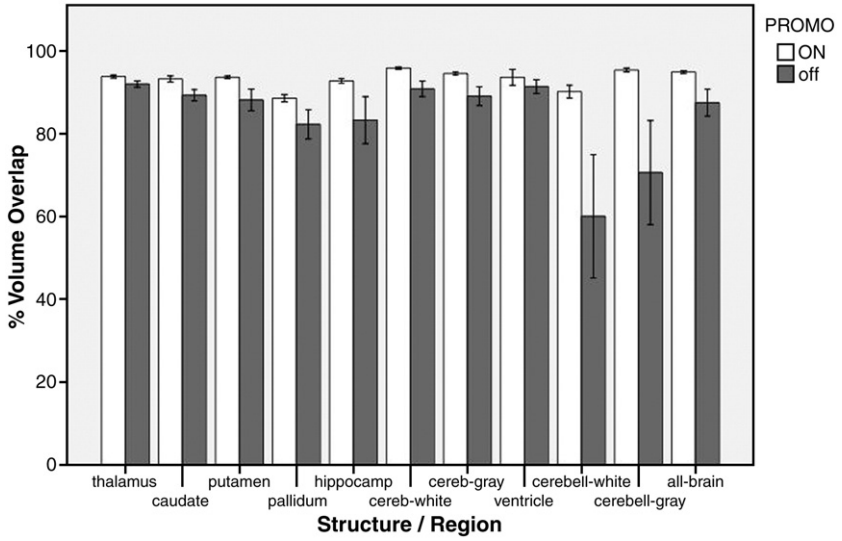

Fig. 3. Comparison of between-scan reliability for automated segmentation with and without motion correction. Percent volume overlap for structures and regions of interest with PROMO motion correction enabled and disabled. Error bars represent ± one standard error of the mean.

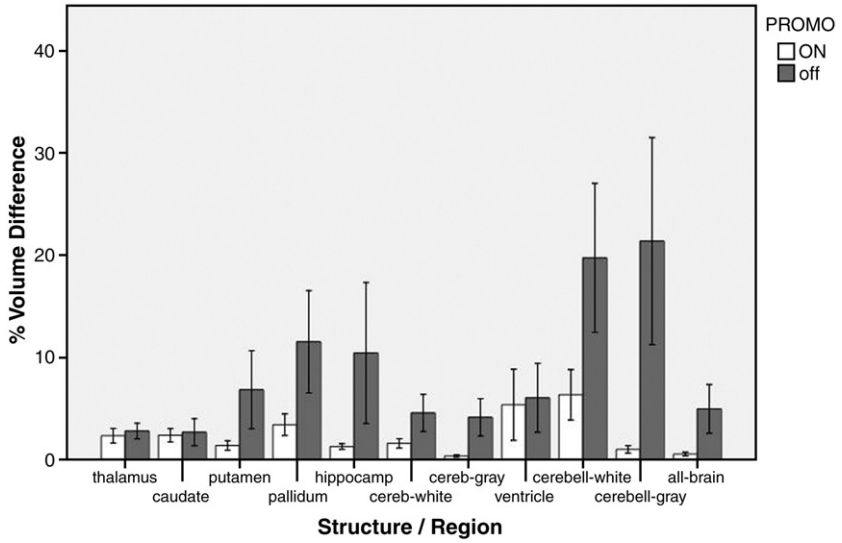

Fig. 4. Comparison of between-scan reliability for automated volumetric measurements with and without motion correction. Percent volume difference for structures and regions of interest with PROMO motion correction enabled and disabled. Error bars represent ± one standard error of the mean.

Discussion

This paper describes the application of a new prospective motion correction technique in magnetic resonance imaging called PROMO that uses interleaved spiral navigator scans and a flexible, image-based position tracking and correction method to reduce 3D rigid-body motion artifacts. The main purpose of the study was to evaluate the effectiveness of PROMO as naturalistically applied to a movement-prone population using several dependent variables that are of primary interest to cognitive neuroscience researchers, including qualitative image quality and clarity, cortical surface reconstruction success, and quantitative subcortical volumetric measures. According to both subjective and objective measures, the use of PROMO during data acquisition consistently improved imaging data quality and reduced artifacts caused by head motion. Notably, all measures that were evaluated showed effects that were in the direction of improvement with the use of motion correction, including better overall image clarity, reduced motion-specific artifacts, and decreased between-scan variability.

Essentially all of the structures and regions of interest we tested showed statistically significant improvements in percent volume overlap with the use of motion correction; thalamus was borderline significant ($p = 0.06$). Percent volume overlap has been used previously (Collins et al., 1995; Fischl et al., 2002) and we believe is an especially sensitive metric of PROMO's ability to measure and adjust for motion as movement occurs, keeping the image coordinate system fixed relative to brain position. Both with and without respect to structure position information, motion most adversely affected volumetric measurements of cerebellar gray and white matter, leading to significantly reduced between-scan replicability in cerebellar volumes. These findings provide a clear example of the importance of reliability in making MRI-based volumetric measurements, since group differences and individual changes in cerebellar size and anatomy have been implicated in a wide range of neurological, psychiatric, developmental, and genetic disorders (e.g., Courchesne et al., 2001; Ho et al., 2004; Millen and Gleason, 2008; Mostofsky et al., 1998; Onodera et al., 1998). Since head motion can be greater in patient populations relative to age-matched control subjects, improvements in the reliability of volumetric measures should help to increase the sensitivity for making neuroanatomical distinctions between groups and should help reduce potential spurious group differences driven by confounding levels of movement. The same cautions and potential improvements hold for developmental and aging studies making cross-sectional and longitudinal comparisons across age (e.g., Brown et al., 2005; Gogtay et al., 2004; Sowell et al., 2003; Walhovd et al., 2005).

For volumes computed without regard to image position overlap, the use of PROMO during acquisition improved the between-scan reliability of volumetric measures particularly well for cerebral gray matter, cerebellar gray and white matter, putamen, and hippocampus. There was essentially no difference in percent volume differences between motion-corrected and uncorrected measures for the thalamus and caudate, structures with strong volumetric measurement reliability even with uncorrected images. The notably greater between-scan variability in uncorrected images for the cerebellum relative to deep, midline cerebral structures might result from greater relative displacement of lateral, caudal, and rostral brain regions during typical head motion in the scanner.

Accurate gray and white matter surface delineation is especially important for the calculation of cortical area, thickness, and curvature (Fischl and Dale, 2000), and images acquired using PROMO successfully completed automated reconstructions in 16 of the 18 volumes, as compared to only seven without correction. Although both cortical surface reconstruction and subcortical volumetric segmentation can be improved with operator guidance and editing, such manual procedures are undeniably more time consuming and less objective.

The magnitude of head motion displayed by our child participants, as measured by navigator scans, was highly variable and often large, typical of children within the grade school age range. The fact that healthy, typically developing children showed norms of up to more than a centimeter of translation and up to 15° of rotation from their original head position clearly demonstrates how perilous movement can be to MRI measurements of the brain, which often depend on sensitivities and distinctions being made at a much smaller scale. We are unaware of any previous work to date that has quantified child head movements in this way. Future pediatric studies, powered by larger sample sizes and a greater age range, might consider examining developmental relationships among maturational factors and specific kinds of motion.

The immense variability in head motion across children contributed to a wide range of scanning durations with the use of PROMO, spanning from no additional time to almost 5 min of scanning beyond the initial 8 min, 40 s required for a non-corrected T1 volume. Even including this particularly rascally individual, average rescan time using PROMO was still just under 35 s per volume and in 10 of the 18 scans was less than 8 s. Despite the inordinate additional acquisition time required for this particular subject, it nevertheless would seem to be a reasonable tradeoff for obtaining data that otherwise would likely be unusable and determined to be so only after completing a standard scan and viewing the reconstructed images. It is worth noting that the rescan threshold can be adjusted for a particular research purpose, clinical protocol, or patient group in order to strike the desired balance between obtaining clear, quantifiable data and minimizing time in the scanner.

In addition to improvements in quantitative measures, PROMO-corrected volumes also were consistently rated subjectively as superior to uncorrected images for both overall clarity and reduced motion-specific artifacts. As with quantitative measures, qualitative ratings were better in all cases when PROMO was enabled. Although this particular study did not focus on clinical pulse sequences, our findings suggest that prospective motion correction would also be useful in standard clinical neuroradiological assessment and diagnosis. To date, PROMO has been implemented in both T1- and T2-weighted 3D pulse sequences at 1.5 and 3 Tesla magnet strengths and also has been used in spectroscopy sequences (Keating et al., in press). In principle, these methods can be applied to a wide variety of imaging purposes, and future applications will include diffusion-weighted, arterial spin labeling (ASL), and blood oxygenation level-dependent (BOLD) sequences. Further evaluation of PROMO might examine its effects on brain activity maps in functional scans, as well as on ratings made by neuroradiologists using images obtained from patients during standard clinical imaging protocols.

Subject and patient head motion during MRI acquisition can significantly impair the ability of scientists and clinicians to detect subtle structural differences and changes associated with brain disease, injury, maturation, and aging. With continued development and refinement, we believe prospective motion correction techniques such as PROMO will significantly improve the accuracy of our qualitative and quantitative measurements for research and clinical care.

Acknowledgments

The authors gratefully thank the children and parents who volunteered to participate in this research. This study was supported by grants from the National Institutes of Health Specialized Neuroscience Research Programs (U54 NS056883), the National Institute on Drug Abuse (RC2 DA029475), the National Institute of Neurological Disorders and Stroke (P50 NS022343), support from General Electric, and by a Fellowship from the UCSD Institute for Neural Computation and an Innovative Research Award from the Kavli Institute for Brain and Mind to Tim Brown.

Appendix A. Supplementary data

Supplementary data associated with this article can be found, in the online version, at doi:10.1016/j.neuroimage.2010.06.017.

References

Blumenthal, J.D., Zijdenbos, A., 2002. Motion artifact in magnetic resonance imaging: implications for automated analysis. Neuroimage 16, 89–92.

Brown, T.T., Lugar, H.M., Coalson, R.S., Miezin, F.M., Petersen, S.E., Schlaggar, B.L., 2005. Developmental changes in human cerebral functional organization for word generation. Cer. Cortex 15, 275–290.

Brown, T.T., Petersen, S.E., Schlaggar, B.L., 2006. Does human functional brain organization shift from diffuse to focal with development? Dev. Sci. 9, 9–11.

Byars, A.W., Holland, S.K., Strawsburg, R.H., Schmithorst, V.J., Dunn, R.S., Ball, W.S., 2002. Practical aspects of conducting large-scale fMRI studies in children. J. Child Neurol. 17, 885–890.

Collins, D., Dai, W., Peters, T., Evens, A., 1995. Automatic 3D model-based neuroanatomical segmentation. Hum. Brain Mapp. 3, 190–205.

Courchesne, E., Karns, C.M., Davis, H.R., Ziccardi, R., Carper, R.A., Tigue, Z.D., Chisum, H.J., Moses, P., Pierce, K., Lord, C., Lincoln, A.J., Pizzo, S., Schreibman, L., Haas, R.H., Akshoomoff, N.A., Courchesne, R.Y., 2001. Unusual brain growth patterns in early life in patients with autistic disorder: an MRI study. Neurol 57, 245–254.

Cox, R.W., Jesmanowicz, A., 1999. Real-time 3D image registration for functional MRI. Magn. Reson. Med. 42, 1014–1018.

Dale, A.M., Fischl, B., Sereno, M.I., 1999. Cortical surface-based analysis I: segmentation and surface reconstruction. Neuroimage 9, 179–194.

Davidson, M.C., Thomas, K.M., Casey, B.J., 2003. Imaging the developing brain with fMRI. Ment. Ret. Dev. Disabil. Res. Rev. 9, 161–167.

Firmin, D., Keegan, J., 2001. Navigator echoes in cardiac magnetic resonance. J. Cardiovasc. Magn. Reson. 3, 183–193.

Fischl, B., Dale, A.M., 2000. Measuring the thickness of the human cerebral cortex from magnetic resonance images. Proc. Natl. Acad. Sci. USA 97, 11050–11055.

Fischl, B., Sereno, M.I., Tootell, R.B.H., Dale, A.M., 1999. High-resolution inter-subject averaging and a coordinate system for the cortical surface. Hum. Brain Mapp. 8, 272–284.

Fischl, B., Liu, A., Dale, A.M., 2001. Automated manifold surgery: constructing geometrically accurate and topologically correct models of the human cerebral cortex. IEEE Trans. Med. Imag. 20, 70–80.

Fischl, B., Salat, D.H., Busa, E., Albert, M., Dieterich, M., Haselgrove, C., van der Kouwe, A., Killiany, R., Kennedy, D., Klaveness, S., Montillo, A., Makris, N., Rosen, B., Dale, A.M., 2002. Whole brain segmentation: automated labeling of neuroanatomical structures in the human brain. Neuron 33, 341–355.

Friston, K.J., Ashburner, J., Frith, C., Poline, J.B., Heather, J.D., Frackowiak, R.S.J., 1995. Spatial registration and normalization of images. Hum. Brain Mapp. 2, 165–189.

Fu, Z.W., Wang, Y., Grimm, R.C., Rossman, P.J., Felmlee, J.P., Riederer, S.J., Ehman, R.L., 1995. Orbital navigator echoes for motion measurements in magnetic resonance imaging. Magn. Reson. Med. 34, 746–753.

Gelb, A., 1974. Applied Optimal Estimation. MIT Press, Cambridge.

Gogtay, N., Giedd, J.N., Lusk, L., Hayashi, K.M., Greenstein, D., Vaituzis, A.C., Nugent, T.F., Herman, D.H., Clasen, L.S., Toga, A.W., Rapoport, J.L., Thompson, P.M., 2004. Dynamic mapping of human cortical development during childhood through early adulthood. Proc. Natl. Acad. Sci. USA 101, 8174–8179.

Ho, B.-C., Mola, C., Andreasen, N., 2004. Cerebellar dysfunction in neuroleptic naive schizophrenia patients: clinical, cognitive, and neuroanatomic correlates of cerebellar neurologic signs. Biol Psychiat 55, 1146–1153.

Irarrazabal, P., Nishimura, D.G., 1995. Fast three-dimensional magnetic resonance imaging. Magn. Reson. Med. 33, 656–662.

Jenkinson, M., Smith, S., 2001. A global optimisation method for robust affine registration of brain images. Med. Image Anal. 5, 143–156.

Jezzard, P., Clare, S., 1999. Sources of distortion in functional MRI data. Hum. Brain Mapp. 8, 80–85.

Keating, B., Deng, W., Roddey, J.C., White, N.S., Dale, A.M., Stenger, V.A., Ernst, T., in press. Prospective motion correction for single-voxel 1H MR spectroscopy. Magn. Reson. Med. doi:10.1002/mrm.22448.

Kochunov, P., Lancaster, J.L., Glahn, D.C., Purdy, D., Laird, A.R., Gao, F., Fox, P., 2006. Retrospective motion correction protocol for high-resolution anatomical MRI. Hum. Brain Mapp. 27, 957–962.

Liu, C., Bammer, R., Kim, D.H., Moseley, M.E., 2004. Self-navigated interleaved spiral (SNAILS): application to high-resolution diffusion tensor imaging. Magn. Reson. Med. 52, 1388–1396.

Malviya, S., Voepel-Lewis, T., Tait, A.R., 1997. Adverse events and risk factors associated with the sedation of children by nonanesthesiologists. Anesth. Analg. 85, 1207–1213.

Manduca, A., McGee, K.P., Welch, E.B., Felmlee, J.P., Grimm, R.C., Ehman, R.L., 2000. Autocorrection in MR imaging: adaptive motion correction without navigator echoes. Radiol 215, 904–909.

Millen, K.J., Gleason, J.G., 2008. Cerebellar development and disease. Curr. Opin. Neurobiol. 18, 12–19.

Mostofsky, S.H., Mazzocco, M.M.M., Aakalu, G., Warsofsky, I.S., Denckla, M.B., Reiss, A.L., 1998. Decreased cerebellar posterior vermis size in fragile X syndrome: correlation with neurocognitive performance. Neurol 50, 121–130.

Norris, D.G., Driesel, W., 2001. Online motion correction for diffusion-weighted imaging using navigator echoes: application to RARE imaging without sensitivity loss. Magn. Reson. Med. 45, 729–733.

Onodera, O., Idezuka, J., Igarashi, S., Takiyama, Y., Endo, K., Takano, H., Oyake, M., Tanaka, H., Inuzuka, T., Hayashi, T., Yuasa, T., Ito, J., Miyatake, T., Tsuji, S., 1998. Progressive atrophy of cerebellum and brainstem as a function of age and the size of the expanded CAG repeats in the MJD1 gene in Machado–Joseph disease. Ann. Neurol. 43, 288–296.

Pipe, J.G., 1999. Motion correction with PROPELLER MRI: application to head motion and free-breathing cardiac imaging. Magn. Reson. Med. 42, 963–969.

Poldrack, R.A., Paré-Blagoev, E.J., Grant, P.E., 2002. Pediatric functional magnetic resonance imaging: progress and challenges. Top. Magn. Res. Imag. 13, 61–70.

Roddey, C., Shankaranarayanan, A., Han, E.T., White, N., Dale, A., 2008. Motion insensitive imaging using 3D PROspective MOtion (PROMO) correction with region-of-interest tracking. ISMRM, Berkeley, USA.

Ronchera-Oms, C.L., Casillas, C., Martí-Bonmatí, L., Poyatos, C., Tomás, J., Sobejano, A., Jiménez, N.V., 1994. Oral chloral hydrate provides effective and safe sedation in paediatric magnetic resonance imaging. J. Clin. Pharm. Ther. 19, 239–243.

Shankaranarayanan, A., Roddey, C., White, N.S., Han, E.T., Rettmann, D., Santos, J., Schmidt, E., Dale, A.M., 2007. Motion Insensitive 3D Imaging Using a Novel Real-Time Image-based 3D PROspective MOtion Correction Method (3D PROMO), Germany. ISMRM, Berkeley, USA.

Sowell, E.R., Peterson, B.S., Thompson, P.M., Welcome, S.E., Henkenius, A.L., Toga, A.W., 2003. Mapping cortical change across the human life span. Nat. Neurosci. 6, 309–315.

Speck, O., Hennig, J., Zaitsev, M., 2006. Prospective real-time slice-by-slice motion correction for fMRI in freely moving subjects. Magma 19, 55–61.

van der Kouwe, A.J., Benner, T., Dale, A.M., 2006. Real-time rigid body motion correction and shimming using cloverleaf navigators. Magn. Reson. Med. 56, 1019–1032.

Voepel-Lewis, T., Malviya, S., Prochaska, G., Tait, A.R., 2000. Sedation failures in children undergoing MRI and CT: is temperament a factor? Paediatr. Anaesth. 10, 319–323.

Walhovd, K.B., Fjell, A.M., Reinvang, I., Lundervold, A., Dale, A.M., Eilertsen, D.E., Quinn, B.T., Salat, D., Makris, N., Fischl, B., 2005. Effects of age on volumes of cortex, white matter and subcortical structures. Neurobiol. Aging 26, 1261–1267.

Ward, H.A., Riederer, S.J., Grimm, R.C., Ehman, R.L., Felmlee, J.P., Jack Jr., C.R., 2000. Prospective multiaxial motion correction for fMRI. Magn. Reson. Med. 43, 459–469.

Weih, K.S., Driesel, W., von Mengershausen, M., Norris, D.G., 2004. Online motion correction for diffusion-weighted segmented-EPI and FLASH imaging. Magma 16, 277–283.

Welch, E.B., Manduca, A., Grimm, R.C., Ward, H.A., Jack Jr., C.R., 2002. Spherical navigator echoes for full 3D rigid body motion measurement in MRI. Magn. Reson. Med. 47, 32–41.

White, N.S., Shankaranarayanan, A., Han, E.T., Gaddipati, A., Roddey, C., Dale, A.M., 2007. Prospective Motion Correction Using Nonlinear Predictive Filtering, Germany. ISMRM, Berkeley, USA.

White, N.S., Roddey, C., Shankaranarayanan, A., Han, E., Rettmann, D., Santos, J., Kuperman, J., Dale, A.M., 2010. PROMO: real-time prospective motion correction in MRI using image-based tracking. Magn. Reson. Med. 63, 91–105.

Wilke, M., Holland, S.K., Myseros, J.S., Schmithorst, V.J., Ball, W.S., 2003. Functional magnetic resonance imaging in pediatrics. Neuroped 34, 225–233.

Wong, S.T., Roos, M.S., 1994. A strategy for sampling on a sphere applied to 3D selective RF pulse design. Magn. Reson. Med. 32, 778–784.

Woods, R.P., Grafton, S.T., Holmes, C.J., Cherry, S.R., Mazziotta, J.C., 1998. Automated image registration: I. General methods and intrasubject, intramodality validation. J. Comput. Assist. Tomogr. 22, 139–152.

Zaitsev, M., Dold, C., Sakas, G., Hennig, J., Speck, O., 2006. Magnetic resonance imaging of freely moving objects: prospective real-time motion correction using an external optical motion tracking system. Neuroimage 31, 1038–1050.